Tracking the structural arrangement of ions in carbon supercapacitor nanopores using in-situ small-angle X-ray scattering

C. Prehal, D. Weingarth, E. Perre, R. T. Lechner,
H. Amenitsch, O. Paris, and V. Presser

Electronic Supplementary Information

A. Charge storage mechanism related to "ion counting"

The following scheme (**Fig. S1**) emphasizes the possible scenarios of cation/anion concentration changes enabling charge balance with the electrode. A similar figure has already been shown by Griffin et al.[1]

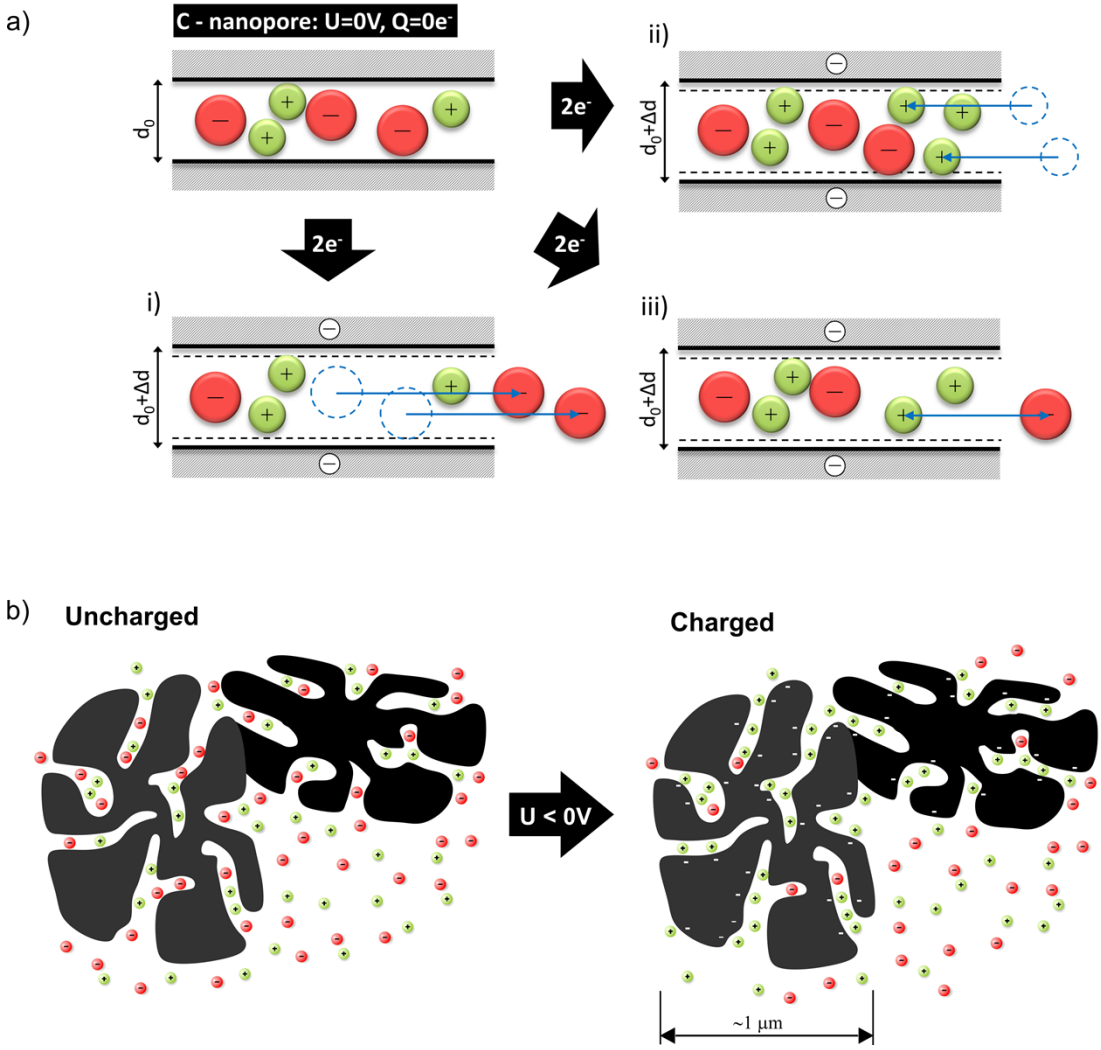

Fig. S1 Possible mechanisms how ions can compensate the electrode charge within a micropore **a**) and on a large scale **b**). Panel **a)** shows i) co-ion expulsion, ii) counter-ion adsorption, and iii) ion swapping (ion exchange). The different mechanisms could also lead to a different pore swelling as indicated. However, pore swelling will not be discussed here further. **b)** The electrode is built up by interconnected activated carbon particles with a size in the µm range. While the surface area of macropores is negligibly small as compared to the surface area of micropores, the volume of micropores and macropores is comparable. While ions are exchanged upon applying a voltage the bulk electrolyte concentration of both ion species remains constant. Note that the double-layer at the outer surface of the carbon particles (interparticulate pores) is not sketched, since its influence on both the electrochemical and the SAXS signal is negligible (mainly due to the small interparticulate surface area).

B. Porosity analysis of the carbon electrode

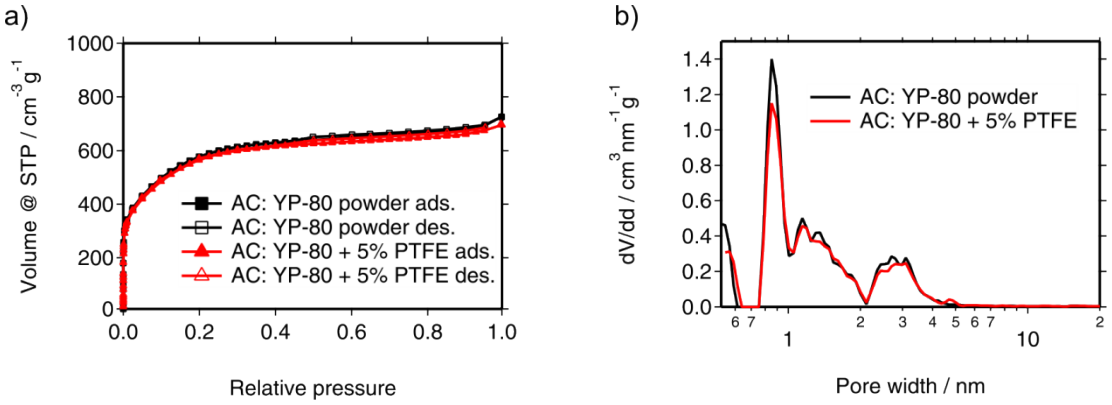

Fig. S2 N_2 sorption isotherm (a) and calculated pore size distribution pattern (b) of activated carbon powders and electrodes. STP: standard temperature and pressure.

Nitrogen gas sorption measurements of the activated carbons (AC) used for the experiments were carried out at -196 °C with an Autosorb iQ system (Quantachrome). The samples were outgassed at 150 °C for 10 h at ca. 100 Pa to remove adsorbed water. Nitrogen gas sorption was performed in the relative pressure range from 10^{-7} to 1.0 in 68 steps. The specific surface area (SSA) was calculated with the ASiQwin-software using the Brunauer-Emmett-Teller (BET) equation[2] in the linear relative pressure range 0.01-0.2. We also calculated the SSA and pore size distribution (PSD) via quenched-solid density functional theory (QSDFT) with a hybrid model for slit and cylindrical pores and pore size between 0.56 and 37.5 nm.[3, 4] The hybrid model yielded a better fit compared to a simple slit-shaped pore model. Values for the total pore volume correspond to p/p_0=0.95. The results are summarized in **Table S1**. The process of electrode fabrication (i.e., powder compaction and addition of polymer binder) reduces slightly the pore volume and the SSA.

Table S1 Results of the gas sorption analysis of the activated carbon (AC) powder and electrode.

	Specific surface area (m^2/g)		Pore volume (cm^3/g)	Volume-weighted average pore size d_{50} (nm)
	BET	DFT		
Powder	2135	1641	1.02	1.3
Electrode	2104	1672	0.99	1.3

C. Transmission concentration calculation

Eqs. 1 & 2 in the main paper were used to calculate the concentration of cations and anions as a function of the applied cell voltage. Here, we describe in more detail how these calculations were performed. Since the working electrode (WE) volume is significantly lower than the one of the counter electrode (CE), the current measured by the potentiostat is determined by the accumulated/depleted charge per time unit of the WE only. Integrating the current signal over time gives the electrosorbed charge at the WE surface. Additionally, the charge is normalized by the electrolyte (pore) volume which was estimated from the transmission value at 0 V as follows. The transmission values were determined for the empty (not soaked) and the electrolyte filled carbon electrode at ambient conditions (around 30% relative humidity). The carbon contribution in ***Eq. 1*** (main paper) is known from the measurement of the non-soaked carbon electrode. Assuming an initial ion concentration of 1 M within the entire electrolyte (pore-) volume at 0 V, d_{el} in ***Eq. 1*** (main paper) can be determined separately, and hence, the electrolyte volume can be calculated. This value may be slightly larger than the actual pore volume since a small electrolyte film might be present also on the outer surface of the electrode. Further errors for the electrolyte volume estimate may occur due to the presence of water within the micropores of the non-soaked carbon at ambient pressure. We account for this error by the error bar evaluation described in the paragraph below. However, the calculated concentration changes (**Fig. S3**) correspond to changes within the entire (global) irradiated electrolyte volume, including electrolyte within all pore size regimes.

The estimated electrolyte volumes within the entire working electrode (300 µm thickness, 11 mm diameter) are shown for all three samples in **Table S2**. The differences in the electrolyte volume of these nominally identical samples might be attributed to a different thickness in a thin electrolyte film wetting the outer electrode surface.

Table S2. Electrolyte volumes within the investigated working electrode (WE) determined for all three samples.

	CsCl	KCl	NaCl
Electrolyte volume [cm^3]	0.027	0.028	0.023

In **Fig. 3** (main paper) all concentration changes are presented in one single plot for comparison, and for the sake of clarity, neither error bars nor the total ion concentrations are shown. In **Fig. S3a-c**, the cation (red) and anion (green) concentration changes are given as a function of the applied charge. Each cation/anion concentration value in **Fig. S3** has been calculated several times using input parameters (***Eqs. 1&2*** in the main paper) varied according to a Gaussian distribution with a reasonably estimated standard deviation. The standard deviations of the resulting cation/anion concentration distribution are shown as error bars in **Fig. S3**; the mean value being the cation/anion concentration. The total ion concentration (sum of cation- and anion concentration) are shown as black data points.

As can be seen, at larger charges the total ion concentration slightly increases; we interpret this as the onset of counter-ion adsorption predominance. However, this effect is rather small as compared to previous eQCMB studies, confirming ion swapping being the major charge compensating mechanism in the present work.[5]

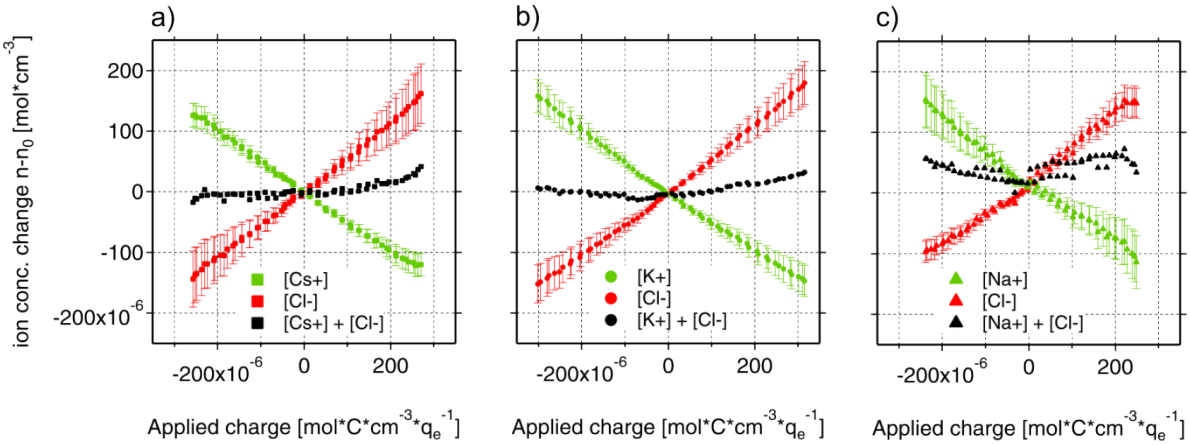

Fig. S3 Cation (green) and anion (red) concentration as a function of applied charge of the a) CsCl, b) KCl, and c) NaCl samples are given as a function of the applied normalized charge. In black the total ion concentration change (cation + anion concentration change) is indicated.

It is generally accepted that ion swapping dominates with respect to counter-ion adsorption at larger initial ion concentrations within the pores and small applied charges.[6] However, it is important to note that due to entropic reasons, a significant amount of co-ions will always be present within the pores at any applied charge. Hence, the co-ion expulsion is expected to saturate at large applied charge or voltage. In all three samples, the onset of such saturation is visible.

D. SAXS and WAXS measurements of carbon soaked in electrolyte

In general, the scattering intensity *I(Q)* corresponds to the Fourier transform of the square of the electron density and can be simplified to ***Eq. S1***, in the case of a 2-phase system consisting of a (carbon) matrix and pores in the small-angle scattering SAXS regime.[7, 8]

$$I_{SAXS}(\vec{Q}) \propto \varphi(1-\varphi) * (\rho_{matrix} - \rho_{pore})^2 * \left| \int_V \Theta(\vec{r})\, e^{-i\vec{Q}\vec{r}} dV \right|^2 \quad \text{(S1)}$$

$\vec{Q}$ is the scattering vector with its modulus for elastic scattering being given by $Q = 4\pi \sin(\theta)/\lambda$, where 2θ is the scattering angle and λ the X-ray wavelength. $\Theta(\vec{r})$ is the Heaviside step function of the system, $\vec{r}$ the distance vector in real space, and V the volume of the sample. Generally, the scattering intensity at high Q-values is related to small features in real space and vice versa. The detailed information is hidden in the integral in ***Eq. S1***, which is usually not known analytically for highly disordered systems such as activated carbons. Beside this term which contains all structural details, the square of the electron density difference $\Delta\rho^2 = (\rho_{matrix} - \rho_{pore})^2$ (scattering contrast), together with the product of the volume fractions of pores (φ) and carbon $(1-\varphi)$, determines the magnitude of the scattering intensity.

In **Fig. S4a**, the scattering intensity for activated carbon (AC) either in air or when soaked with 1 M NaCl is shown at 0 V for a scattering vector length Q from 0.3 to 20 nm^{-1}. In addition to the SAXS signal shown in the main paper (Q-range from 0.3-8 nm^{-1}) we include here also the so called wide-angle X-ray scattering (WAXS) (Q-range from 9.5-20 nm^{-1}) which was measured by an additional detector simultaneously with the SAXS signal.

The WAXS intensity of the AC with 1 M aqueous NaCl includes the carbon structure factor (002)-peak (visible for "AC in air") and the first water structure factor peak around 20 nm^{-1}.[9] Generally, the scattering intensity can be described by the sum of the atomic/molecular structure factor and the two-phase model SAXS intensity.[8, 10] Moreover, both the electrolyte and the carbon structure factor become roughly constant at low Q-values in the SAXS regime (Q < 8 nm^{-1}), as indicated by the horizontal dashed lines in **Fig. S4a**. Besides the water structure factor itself, the electrolyte structure factor is assumed to be determined by the diffuse scattering from randomly distributed ions within the water matrix (similar to the so-called Laue scattering concept, known from solid solutions)[10]. Hence, the height of the electrolyte structure factor contribution in the SAXS regime depends uniquely on the ion concentration as explained in more detail in section E below. In **Fig. S4b** the SAXS intensity for all three electrolytes is shown. Note the difference in intensity in particular at larger Q-values (Q > 5nm^{-1}: electrolyte structure factor).

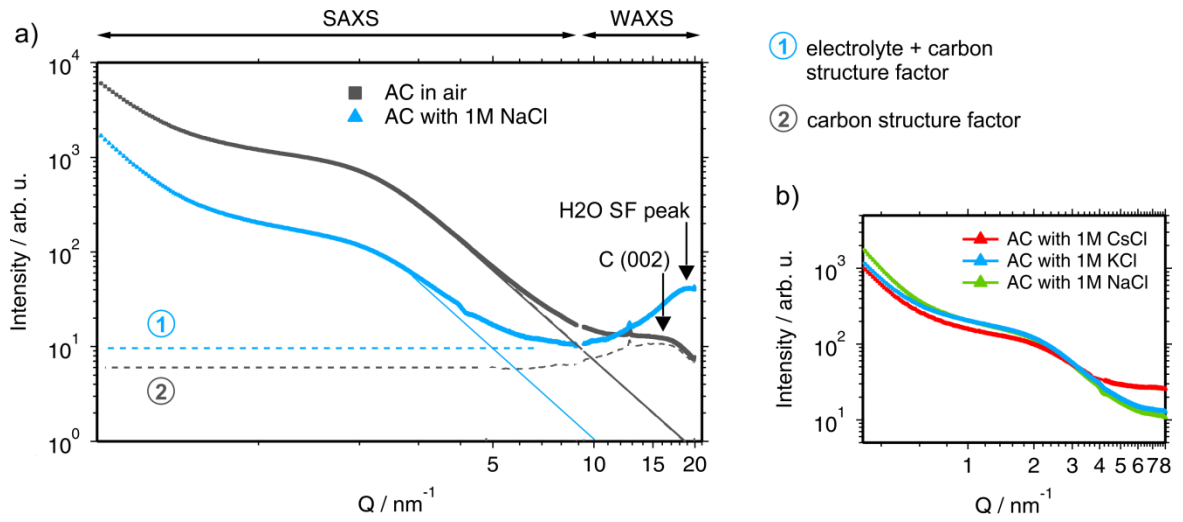

Fig. S4 **a)** SAXS and WAXS intensity for the activated carbon in air (grey) and filled with a 1M NaCl electrolyte (blue). The thin (grey and blue) lines indicate the power law decay of the SAXS intensity at larger Q-values. The horizontal dashed lines (both blue and grey) indicate the constant contribution of the carbon and electrolyte structure factors in the SAXS regime. **b)** SAXS intensity for the AC filled with three different electrolytes: 1 M CsCl, 1M KCl, NaCl. The scattering curves were measured at 0 V cell potential within the in-situ cells used for the measurements shown in **Fig. 4**, main paper.

E. Scattering from a liquid: the electrolyte structure factor

Since the atomic structure of AC is not correlated to the atomic/molecular structure of the liquid electrolyte, the two structure factor contributions are additive and can be treated separately. As we discuss only relative changes of the SAXS intensity in this work, the constant AC structure factor does not need to be taken into account in the following discussion of the electrolyte structure factor.

The scattering cross section (being proportional to the measured intensity) of an aqueous electrolyte consisting of cations, anions and water molecules can be expressed by ***Eq. S2***.[11, 12]

$$\frac{d\Sigma}{d\Omega}(Q) * V = \sum_{\alpha} \gamma_{\alpha} {f_{\alpha}}^2 + \sum_{\alpha} \sum_{\beta \geq \alpha} (2 - \delta_{\alpha\beta}) \phi_{\alpha} \phi_{\beta} f_{\alpha} f_{\beta} [S_{\alpha\beta} - 1] \quad , \qquad \text{(S2)}$$

$S_{\alpha\beta}$ represent the partial structure factors which cover the cross-correlations of species α with species β. f and ϕ are the atomic/molecular formfactors and the number fractions, respectively, and $\delta_{\alpha\beta}$ is the Kronecker delta ($\delta_{\alpha\beta} = 0 \; for \; \alpha \neq \beta; \delta_{\alpha\alpha} = 1$). At small scattering angles the atomic/molecular form factors can be replaced by the respective electron numbers n. For a random distribution of the ions within the solvent, the ion-ion partial structure factors can be set to 1. Although a 1 M solution is not dilute, the ratio between the number of water molecule per cation/anion is high enough to make the following additional approximations: $\phi_{H2O} \cong 1$, $1 - \phi_{an} \cong 1$, $1 - \phi_{cat} \cong 1$, $1 - \phi_{H2O} \cong \phi_{cat} + \phi_{an}$ and $\phi_{cat}\phi_{an} \cong 0$.

With this, ***Eq. S2*** simplifies to ***Eq. S3***:

$$\frac{d\Sigma}{d\Omega}(Q) * V \cong \phi_{cat}\left[(n_{cat} - n_{H_2O})^2 + 2n_{cat}n_{H_2O}S_{catH_2O}\right]$$

$$+ \phi_{an}\left[(n_{an} - n_{H_2O})^2 + 2n_{an}n_{H_2O}S_{anH_2O}\right] + {n_{H_2O}}^2 S_{H_2OH_2O} \quad \text{(S3)}$$

The last term corresponds to the water structure factor. The first two terms depend on the cation and anion concentrations respectively. Changes of the water-water correlation (S_{H2OH2O}) and water-ion correlations (S_{catH_2O}, S_{anH_2O}) are assumed to be small in the SAXS regime. Moreover one can assume that the partial structure factors within the SAXS regime are much smaller than 1. Hence, ***Eq. S3*** can be further simplified to

$$\frac{d\Sigma}{d\Omega}(Q) * V \cong \phi_{cat}(n_{cat} - n_{H_2O})^2 + \phi_{an}(n_{an} - n_{H_2O})^2 + {f_{H2O}}^2 S_{H_2OH_2O}. \quad \text{(S4)}$$

The approximation ***Eq. S4*** shows that the electrolyte structure factor is reduced to the diffuse scattering contribution of non-correlated ions within a water matrix (similar to the so-called Laue scattering in solid solutions)[10] and the water structure factor. From the SAXS data discussed in the main paper it becomes clear that the bare electron numbers of cations and anions cannot explain the observed intensity changes when assuming ion swapping. Only when considering the ions together with a specific number of water molecules in their hydration shell (having a different density as compared to the bulk water) we are able to describe the scattering intensity changes of the region Q-B (shown in **Fig. 4c-d**, main paper). Levi et al.[13] have evaluated a number of tightly bounded water molecules for ions of aqueous electrolytes within different nanoporous carbons using an electrochemical quartz crystal microbalance (eQCM) device. The activated carbon YP-17 used in their studies is comparable to our activated carbon YP-80. Taking the number of tightly bounded water molecules into account, all cations have a larger effective electron number than the anion (Cl^-), shown in **Table S3**. Beside a partial desolvation of ions within confinement in particular the replacement of pore water molecules by the hydrated ions seem to be responsible for the rather low number of tightly bounded water molecules.[13] If a hydrated ion enters the pore, some water molecules simultaneously have to leave the pore, assuming a constant electrolyte volume during adsorption and desorption. Consequently the number of tightly bounded water molecules can be seen as an effective value which is related to the water density within the hydration shell. The increased density of water within the solvation shell of ions with large charge to size ratio was recently shown in a SAXS study of aqueous bulk electrolytes.[14]

Table S3. Parameters of all ions determining their effective electron numbers.

	Cs^+	K^+	Na^+	Cl^-	H_2O
electron number *n* (of bare ion, molecule)	54	18	10	18	10
Tightly bounded H_2O according to Levi et al. [13]	0.5	1.3 (2.2)	2.2 (3)	0.6	-
Effective electron number n_{eff}	59	31 (40)	32 (40)	24	10

The numbers within the brackets are empirically estimated numbers in order to obtain quantitative agreement between the simulated scattering intensity changes and the corresponding experimental data (see **Fig. 6b-d**, main paper and section F below).

F. Calculation of the simulated scattering intensity

The so-called Debye-Anderson-Brumberger (DAB)[15] model represents an analytical expression describing the scattering of random pore systems with an exponentially decaying correlation function. The corresponding scattering cross section is analytically given by ***Eq. S5***:

$$\frac{d\Sigma}{d\Omega}(Q) = \frac{2\pi(\Delta\rho)^2 * S}{(\frac{6}{R_g^{\,2}} + Q^2)^2 * V} \tag{S5}$$

, where R_g corresponds to the radius of gyration, $(\Delta\rho)^2$ to the electron density contrast and S/V to the surface to volume ratio of the pore structure. In the case of activated carbons an additional term has to be considered, covering the contribution of the significant volume of large pores in between the carbon particles, leading to a power law behavior of the intensity at small Q.[16] For fitting the measured scattering intensity the following expression was used (***Eq. S6***):

$$I_{fit}(Q) = \frac{A}{Q^{3.5}} + \frac{B}{(\frac{6}{R_{g,0}^{\,2}} + Q^2)^2} + C \tag{S6}$$

with *A*, *B*, and *C* together with $R_{g,0}$ being fit parameters. The first term corresponds to the contribution of the carbon particles which was found to decay with a power law exponent of -3.5 from a fit of the SAXS intensity of dry AC at low Q-values. The second term corresponds to the micropore scattering (DAB-model), and the third term covers the Q-independent contributions of the electrolyte structure factor and the carbon structure factor. We can split the parameter *C* into the carbon structure factor contribution *BG* (known from measurements of the bare AC, see **Fig. S4a**) and the electrolyte

structure factor contribution $I_{El,0}$. In **Fig. S5a**, the fit is shown for the CsCl sample at 0 V. Although the fit is not perfect, the model covers the basic features of the system which allows simulating the relative intensity changes of the scattering curves as observed from the experimental data in **Fig. 4c-e** in the main paper. The input is given by the relative changes of the radius of gyration $R_{g,0}$ and the electrolyte structure factor $I_{El,0}$ from the SAXS data, and the electron density contrast $(\Delta\rho)^2$ between micropores and carbon matrix calculated from the known concentrations from XRT and the effective electron numbers in Table S3. To this end, ***Eq. S6*** was rewritten as ***Eq. S7***:

$$I_{sim}(Q) = \frac{A}{Q^{3.5}} + \frac{(\Delta\rho)^2{}_{rel} * B}{\left(\frac{6}{R_{g,rel}{}^2 * R_{g,0}{}^2} + Q^2\right)^2} + I_{El,rel} * I_{El,0} + BG \quad (S7)$$

The parameters *A*, *B* and *BG* are kept constant for all simulated scattering curves. *A* and *B* are known from the fit at 0 V (**Fig. S5a**) and *BG* corresponds to the carbon structure factor evaluated from the scattering intensity of the bare AC ("AC in air", **Fig. S4a**). Changes of all other parameters are considered by multiplying a relative value ($(\Delta\rho)^2{}_{rel}$, $R_{g,rel}$, $I_{El,rel}$) to the initial parameters at 0V (B, $R_{g,0}$, $I_{El,0}$).

The electrolyte structure factor contribution $I_{El,rel}$ is calculated according to ***Eq. S4*** in section E using the ion concentration from the transmission calculations and the effective electron numbers of the cations $n_{eff,cat}$ and anions $n_{eff,an}$ (**Table S3**) as an input. In order to obtain relative changes these values are normalized by the value at 0V.

The electron density contrast change $(\Delta\rho)^2$ is estimated by assuming ion concentration changes c_i within the micropores proportional to the calculated ones (**Fig. S3**). The global ion concentration changes calculated from the XRT evaluation cover changes within the entire electrolyte volume of the WE including both macropores and micropores. Due to the low macropore surface area all concentration changes can be reduced to changes within the micropores. Hence the actual micropore concentration change has to be multiplied by a factor corresponding to the ratio of total to micropore volume $\phi_{total}/\phi_{micro}$. The total pore volume is estimated from the transmission measurement at 0V (section C) and the micropore volume from the gas sorption measurements (section B). The carbon matrix electron density ρ_c is estimated by comparing the height difference between the SAXS intensity (intermediate regime) of the AC in air with the AC infiltrated with electrolyte at 0V. Hence the electron density difference shown in **Fig. S5b** is written as ***Eq. S8***:

$$(\Delta\rho)^2{}_{rel} = \left(\rho_c - \left(\frac{\phi_{total}}{\phi_{micro}} c_{cat} n_{eff,cat} + \frac{\phi_{total}}{\phi_{micro}} c_{an} n_{eff,an} + c_{H_2O} n_{eff,H_2O}\right)\right)^2 / (\Delta\rho_0)^2 \quad (S8)$$

All time (or voltage) dependent parameters needed as an input for the simulations are shown exemplarily for CsCl in **Fig. S5b**. The resulting simulated scattering curves for all electrolytes are given in **Fig. 6b-d**, main paper.

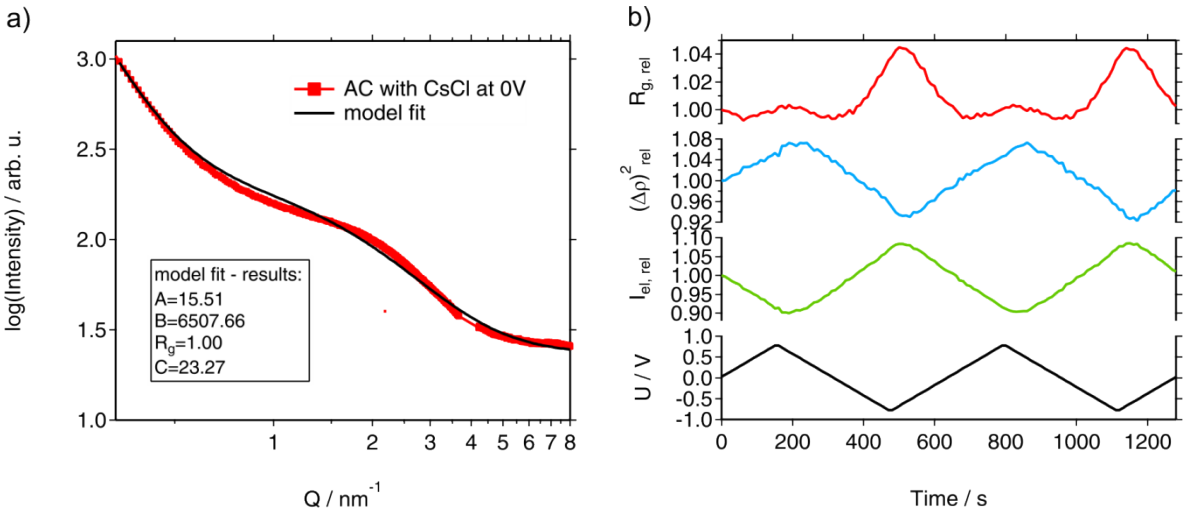

Fig. S5 In a) the SAXS intensity of the AC filled with the 1M CsCl electrolyte at 0V is given (red data points). In black the model fit according to Eq. S7 is indicated. In b) the changing parameters needed for the simulation of the relative CsCl scattering intensity according to equation S7 are shown. The result of the simulation is shown in Fig. 6b (main paper).

References

1 J. M. Griffin, A. C. Forse, H. Wang, N. M. Trease, P.-L. Taberna, P. Simon and C. P. Grey, *Faraday Discuss.*, 2014, **FD 176**.

2 S. Brunauer, P. H. Emmett and E. Teller, *J. Am. Chem. Soc.*, 1938, **60**, 309-319.

3 G. Y. Gor, M. Thommes, K. A. Cychosz and A. V. Neimark, *Carbon*, 2012, **50**, 1583-1590.

4 A. V. Neimark, Y. Lin, P. I. Ravikovitch and M. Thommes, *Carbon*, 2009, **47**, 1617-1628.

5 M. D. Levi, G. Salitra, N. Levy, D. Aurbach and J. Maier, *Nat. Mater.*, 2009, **8**, 872-875.

6 P. M. Biesheuvel, S. Porada, M. Levi and M. Z. Bazant, *J. Solid State Electr.*, 2014, **18**, 1365-1376.

7 O. Glatter and O. Kratky, *Small angle X-ray scattering*, Academic Press Inc. Ltd., London, 1982.

8 J. Als-Nielsen and D. McMorrow, in *Elements of Modern X-ray Physics*, John Wiley & Sons, Inc., 2011, pp. 113-146.

9 M. Bellissent-Funel, *J. Phys.: Condens. Matter*, 2001, **13**, 9165.

10 A. Guinier, *X-ray diffraction in crystals, imperfect crystals, and amorphous bodies*, Courier Dover Publications, 1994.

11 G. Neilson, *Pure Appl. Chem.*, 1988, **60**, 1797-1806.

12 D. T. Bowron and S. Diaz Moreno, *Coord. Chem. Rev.* , 2014, **277–278**, 2-14.

13 M. D. Levi, S. Sigalov, D. Aurbach and L. Daikhin, *J. Phys. Chem. C*, 2013, **117**, 14876-14889.

14 I. Waluyo, C. Huang, D. Nordlund, U. Bergmann, T. M. Weiss, L. G. M. Pettersson and A. Nilsson, *J. Chem. Phys.*, 2011, **134**, 1-10.

15 P. Debye, H. R. Anderson and H. Brumberger, *J. Appl. Phys.*, 1957, **28**, 679-683.

16 A. Gibaud, J. S. Xue and J. R. Dahn, *Carbon*, 1996, **34**, 499-503.